

Investigating the physicochemical properties of solid dispersions based on semicrystalline carriers: A case study with ketoprofen

Serena Bertoni, Beatrice Albertini, Nadia Passerini*

Department of Pharmacy and BioTechnology, PharmTech Lab, Alma Mater Studiorum-University of Bologna, Via S. Donato 19/2, 40127 Bologna, Italy

ARTICLE INFO

Keywords:

Drug carrier miscibility
Drug carrier interactions
Crystallization
Solubility enhancement
Physical stability
Melting process

ABSTRACT

Hydrophilic semicrystalline carriers represent an alternative to amorphous polymers due to their low melting temperature, useful for the production of solid dispersions (SDs) by melting-based technologies. This research aims to compare SDs of ketoprofen (KET) and three different semicrystalline carriers (PEG, Poloxamer and Gelucire) regarding miscibility, phase behavior, molecular interactions and stability. KET was chosen owing to its low solubility and high glass forming ability. Estimation of drug-excipient miscibility was performed by Flory-Huggins theory. Negative Gibbs free energy indicated a spontaneous mixing of KET with the three carriers and miscibility in the order PEG > Poloxamer > Gelucire. SDs up to 40 % w/w of drug were produced by melting process at a temperature below KET melting point. Characterization of SDs was performed by differential scanning calorimetry, polarized light microscopy and powder X-ray diffraction. In case of PEG and Poloxamer, the drug incorporation did not affect carrier crystallinity, while KET was in the amorphous state. Differently, KET retarded the crystallization of Gelucire and at high drug loadings the SDs were amorphous and semisolid. FT-IR analysis revealed a strong interaction between KET and the three carriers. Finally, PEG-based SDs above 20 % KET loading displayed drug crystallization after 6 months of storage; while Poloxamer and Gelucire-based SDs showed KET crystallization only at 40 % KET. Due to its less hydrophilic character and limited water uptake, Gelucire showed the best stability among the three excipients.

1. Introduction

Over the last decades, the strategy of dispersing the active pharmaceutical ingredient (API) within a polymer matrix to form a solid dispersion (SD) has been successfully used to overcome the limited solubility and dissolution rate of poorly water-soluble compounds, as those belonging to class II or IV of the BCS (Leuner and Dressman, 2000). The bioavailability advantage of SDs relies on the transformation of a crystalline raw material into a higher energy physical state, i.e. amorphous form. Reduction of drug particle size to the minimum, larger surface area and increased wettability by the presence of a hydrophilic carrier are additional aspects that favor drug dissolution.

From a structural perspective, the hydrophilic carrier used in pharmaceutical SDs can be amorphous, semi-crystalline or crystalline. Amorphous polymers (e.g. PVP, HPMC, Soluplus) have a random disorganized structure and, since the introduction of SDs, have been the most used type of matrix-forming carrier. Differently from either amorphous polymeric carriers and pure crystalline carriers (e.g. urea, sugars), semicrystalline materials are defined as “carriers containing

both crystalline and amorphous domains, the proportions of which depend on the molecular weight of the carrier and the sample preparation conditions” (Van Duong and Van den Mooter, 2016). Typical examples of hydrophilic semicrystalline polymers with pharmaceutical applications are polyethylene glycols (PEGs), Poloxamers and hydrophilic Gelucires. Although these materials are not currently the first choice excipients to formulate SDs, they have great potential as highly cost-effective and non-toxic alternatives to amorphous polymers (Bertoni et al., 2020; Van Duong et al., 2015; Van Duong and Van den Mooter, 2016). Semicrystalline carriers are suitable to be processed by solvent-free manufacturing technologies such as hot melt extrusion, melt granulation and spray congealing (Alshehri et al., 2020; Bertoni et al., 2019b). Due to their organized and packed molecular structure, they exhibit defined melting points, which are often below 80 °C, lower compared to the glass transition temperature (generally above 100 °C) of amorphous polymers. This allows to use a particularly low process temperature, with advantages from the energetic and environmental points of view.

SDs based on semicrystalline carriers are complex, as both the API

* Corresponding author.

E-mail address: nadia.passerini@unibo.it (N. Passerini).

<https://doi.org/10.1016/j.ijpharm.2022.122576>

Received 6 September 2022; Received in revised form 28 December 2022; Accepted 29 December 2022

Available online 31 December 2022

0378-5173/© 2022 Elsevier B.V. All rights reserved.

and the excipient may present amorphous and crystalline phases (Yang and Gogos, 2013) and the mutual influence on each other determines the properties of the final system. A recent review from Van den Mooter's research group (Van Duong and Van den Mooter, 2016) nicely illustrates the different aspects accounting for the complexity of SDs based on semicrystalline polymers. These aspects include, first of all, the modality of polymer crystallization during the SD solidification. To this regard, Taylor's research group (Zhu et al., 2012) studied the crystallization of various API/PEG dispersions prepared by comelting of the mixture above the melting temperature followed by quick cooling. The results showed that, upon cooling together with the semicrystalline carriers, the crystallization rate of benzocaine decreased, those of ibuprofen and fenofibrate accelerated and finally that of haloperidol was unchanged compared to the pure materials. These findings confirmed that the carrier can accelerate, slow down, or have no influence on the crystallization process of the API during melt processing of SDs. Moreover, it should be noted that not only the API can be subjected to modification by the presence of a semicrystalline polymer, but the carrier can be influenced as well. For example, indomethacin was noted to act as powerful crystallization inhibitor of PEG (Van Duong et al., 2015).

Secondly, depending on how the API incorporates into the semicrystalline structure of the carrier, SDs can be of various physical nature. In some cases, a certain amount of API gets molecularly dissolved in the crystalline polymer and the resultant system is a single-phase (Nair et al., 2020). It has been reported, for example, that oxazepam at 5 % w/w dissolved in PEG forming a solid solution when the system is produced by comelting at a temperature (150 °C) that allowed the solubilization of drug particles in the carrier (Ginés et al., 1996). Alternatively, SDs prepared with semicrystalline materials can be two-phases dispersions with both drug and polymer in the crystalline state, as the case in eutectic or monotectic systems (Abdelkader et al., 2014; Baird and Taylor, 2011).

Despite the remarkable progress in research on pharmaceutical SDs, the API-carrier miscibility, the crystallization mechanism and phase behavior in semicrystalline SDs remain challenging to investigate. These fundamental features of semicrystalline carrier-based dispersions are deeply interconnected; however, in most cases they have been investigated individually, making the literature on this topic rather scattered and lacking of an all-over understanding of the potential and limitations of these formulations. Moreover, most of these aspects have been studied almost exclusively on PEG-based systems, and a comparison between different semicrystalline materials is missing.

Therefore, this research aims to investigate multiple aspects of SDs containing ketoprofen (KET) and three different semicrystalline carriers. These aspects include miscibility, solubility, phase behavior, crystallization, molecular interactions and physical stability. The understanding of how each semicrystalline carrier influences these properties could help in developing efficient manufacturing of novel SDs formulations using these materials.

KET, a non-steroidal anti-inflammatory drug belonging to BCS class II, is a low melting point drug with high glass forming ability (Panini et al., 2019) and able to plasticize both hydrophilic and hydrophobic polymers (Blasi et al., 2020; Gue et al., 2015; Gue et al., 2013). Moreover, the presence of the carboxylic group of KET is potentially able to stabilize intermolecular interactions with hydrophilic groups of the semicrystalline carriers. These interactions might change the polymer's chemical, physical and structural behaviour.

Specifically, the three selected carriers represent the three most common classes of semicrystalline hydrophilic materials with pharmaceutical application: i.e. polyethylene glycol 4000 (PEG), high-Hydrophilic Lipophilic Balance (HLB) Gelucires (Gelu), and Poloxamer 188 (Polox). They differ in their chemical composition (Fig. 1) as well as molecular weight, HLB and surfactant properties. Owing to their melting temperatures in the range 50–70 °C, they can be easily transformed into SDs employing a melting process carried out at a temperature below the KET melting point. Specifically, the excipients were evaluated with regard to their ability to solubilize KET upon melting and their thermodynamic miscibility with the drug by calculation of Flory-Huggins interaction parameters by the melting point depression approach. The physical state and microstructure of SD with drug content ranging from 10 to 40 % w/w were characterized using Differential Scanning Calorimetry (DSC), Polarized Light Microscopy (PLM) and powder X-ray diffraction (PXRD). Additionally, the formation of intermolecular interactions between KET and carriers was assessed by FT-IR.

2. Materials and methods

2.1. Materials

Ketoprofen (KET) and polyethylene glycol (PEG) 4000 were purchased from Sigma Aldrich (Steinheim, Germany). Kolliphor® P188 (Poloxamer 188) was a gift of BASF. Gelucire®50/13 and Gelucire®48/16 were kindly supplied from Gattefossè (Milan, Italy).

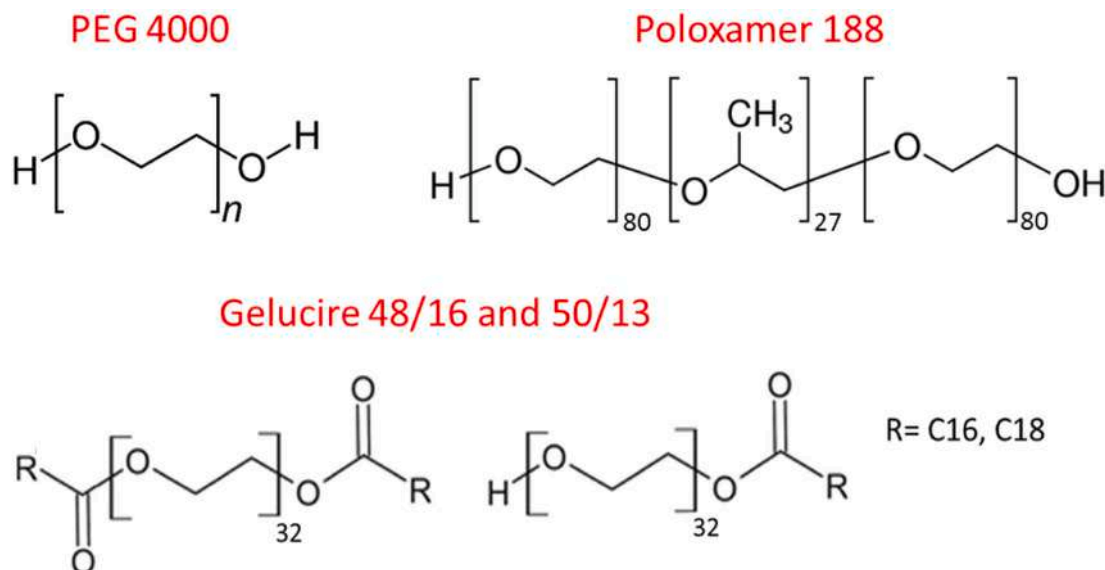


Fig. 1. Chemical structure of the three semicrystalline carriers used.

2.2. Methods

Physical mixtures preparation.

Three semicrystalline carriers were selected, belonging to different classes:

-Polyethylene glycol (PEG): PEG 4000 (micronized powder) was used as received;

-Gelucire (Gelu): since Gelucires® are commercialized as large pellets, spray congealing (Bertoni et al., 2018) was used as fast and solvent-free technology to transform this excipient in form of powder with size 50–200 µm. In order to allow the obtaining of a free-flowing powder completely solid at room temperature, two commercial Gelucire with high HLB values (Gelucire®50/13 and Gelucire®48/16) were mixed at 1:1 wt ratio. This mixture has been previously used as carrier for improving bioavailability of poorly water soluble drugs with positive outcome (Bertoni et al., 2019a);

-Poloxamer (Polox): Kolliphor® P188 was grinded with mortar and pestle until powder of 50–200 µm was obtained;

The properties of the carriers and KET are summarized in Table 1. Physical mixtures (PM) of KET and carriers at various weight ratios were prepared with all carriers by accurately weighing the powders and geometric mixing in an agate mortar using an agate pestle until a homogeneous mixture was obtained. Physical mixtures were used for the DSC analysis.

2.3. Sds preparation

SDs were prepared by melting method in batches of 1 g at a working temperature (70 °C) above the melting temperature of the carrier, but below that of the drug. The weighted amount of carrier was heated up to 70 °C until complete melting, then the appropriate amount of KET was added to the molten carrier. The sample was kept at that temperature for 30 min under magnetic agitation and then cooled to room temperature. SDs were stored in closed glass vials at 25 °C.

2.4. Differential scanning calorimetry (DSC)

DSC analysis was performed with a Perkin-Elmer DSC 6 (Perkin Elmer, Beaconsfield, UK). Before measurements, the instrument was calibrated with indium and lead for the temperature, and with indium for the enthalpy. Six to ten milligrams of sample were placed into aluminum pans and analyzed by DSC under a nitrogen flow of 20 mL/min. DSC analysis were used for:

-Melting point depression and phase diagram by thermal analysis. Pure KET and PM at different compositions (95 %, 90 %, 85 %, 80 %, 75 %, 70 % and 65 % w/w KET) were held isothermally for 1 min, then heated from 25 to 110 °C at a scanning rate of 1 °C/min. The onset (T_{on}), peak (T_{peak}) and end (T_{end}) temperature of melting endotherm of KET was recorded. Each run was performed in triplicate.

-Thermal behaviour of SDs. SDs were analysed by DSC in order to investigate the physical state of both components. SD were held isothermally for 1 min, then heated from 25 to 120 °C at a scanning rate of 5 °C/min. Pure carriers either as powder (raw materials) or after been crystallized from the melt were analysed using the same protocol.

-Crystallization behaviour of SDs. To investigate the effect of KET on

Table 1

Properties of ketoprofen and semicrystalline carrier used.

	Ketoprofen (KET)	PEG	Poloxamer	Gelucire
Mw (g/mol)	254.28	4000 ^a	8400 ^a	1506 ^a
T_m (°C) ^b	94.18 ± 0.32	66.61 ± 0.34	57.42 ± 0.91	49.11 ± 0.63
ΔH_f (J/g) ^b	112.0 ± 0.28	188.42 ± 0.89	140.29 ± 1.59	134.70 ± 1.49
Density (g/cm ³)	1.28 ^c	1.20 ^a	1.06 ^a	0.90 ^a
Molecular volume (cm ³ /mol)	198.66	3333.33	7924.53	1673.67 ^a

^aaverage value; ^bobtained from the supplier; ^cmeasured by DSC analysis at 10 °C/min (mean ± SD from three measurements); ^cfrom (Baird et al., 2010b).

crystallization, SDs were melted at 70 °C, held isothermally for 5 min, cooled from 65 to 25 °C at a scanning rate of 2 °C/min and then reheated at 1 °C/min to verify the physical form crystallized upon.

2.5. Calculation of interaction parameter by melting point depression approach

The melting point depression method uses the Flory-Huggins interaction parameter theory to calculate the interaction parameter χ . The melting point depression of the drug in the presence of a carrier can be related to χ as follows:

$$\left(\frac{1}{T_{m\text{ mix}}} - \frac{1}{T_{m\text{ drug}}} \right) = \frac{-R}{\Delta H_{fus}} \left[\ln \phi_{drug} + \left(1 - \frac{1}{m} \right) \phi_{polymer} + \chi \phi_{polymer}^2 \right] \quad (1)$$

Where $T_{m\text{ mix}}$ and $T_{m\text{ drug}}$ are the melting temperature of the drug in presence and in absence of the carrier, respectively. R is the gas constant ($R = 8.314 \text{ J K}^{-1} \text{ mol}^{-1}$), ΔH_{fus} is the heat of fusion of the pure drug, m is the ratio of the volume occupied by the carrier to that occupy by the drug, ϕ_{drug} and $\phi_{polymer}$ are the volume fractions of the drug and the polymer, respectively, in the binary mixture.

The melting point depression was evaluated by DSC analysis. The experimentally obtained values of the onset of melting of KET in the PM were incorporated into the Eq. (1) in order to calculate the χ value for KET and each carrier. By plotting the equation versus $\phi_{polymer}^2$, the slope of the line gave the value of interaction parameter χ .

The free energy of mixing of a drug-carrier binary system, i.e. ΔG_{mix} is described by Eq. (2):

$$\frac{\Delta G_{mix}}{RT} = n_{drug} \ln \phi_{drug} + n_{polymer} \ln \phi_{polymer} + n_{drug} \phi_{polymer} \chi \quad (2)$$

where n_{drug} and $n_{polymer}$ are the number of moles of drug and carrier, respectively and χ is the Flory-Huggins interaction parameter between drug and carrier. ΔG_{mix} in the equation is normalized by gas constant R and absolute temperature T .

2.6. Phase diagrams

Phase diagrams were constructed by plotting the melting temperature (T_{end}) of the first endothermic event of DSC curves of the drug-carrier mixtures. As for the KET melting curves, both the experimental T_{onset} and the T_{end} of melting point depression data were plotted. Moreover, the calculated interaction parameters were introduced into Eq. (1) to estimate T_{mix} for mixtures with different mass ratios, and allowing the melting curves to be extrapolated to lower temperatures (Altamimi and Neau, 2016; Lin and Huang, 2010).

2.7. Evaluation of KET solubility in molten carriers

Carriers were melted and maintained at 70 °C with magnetic agitation. KET was added as powder to the excipient in discrete additions of 5–10 mg. After each addition, the sample was visually inspected to check the presence of undissolved KET powder. The total amount of KET added which completely dissolved was used to calculate the solubility of KET in the molten carriers (at 70 °C) as followed:

$$KET \text{ solubility in the molten carrier} = \frac{KET \text{ added}(mg)}{KET \text{ added}(mg) + \text{carrier}(mg)} \times 100 \quad (3)$$

2.8. Polarized optical microscopy

Microscopy experiments were performed using a Nikon Eclipse E400 polarizing optical microscope equipped with a Mettler-Toledo (Novate Milanese, Italy) hot stage apparatus and a Nikon Digital Net Camera DN100 camera for image acquisition. For this analysis, SD were formed directly on glass slide: SD samples were placed onto a glass slide, heated to 70 °C and held for 5 min in order to obtain an isotropic melt, then covered with a coverslip, resulting in a thin film of sample and finally cooled to room temperature. The slides containing the thin layer of SD were imaged immediately after solidification, after 1 month and 6 months of storage at 25 °C.

2.9. Powder X-ray diffraction (PXRD)

X-ray powder diffraction analysis were performed using an X'Pert powder diffractometer (Malvern Panalytical, Almelo, NL, USA) equipped with a graphite monochromator in the diffracted beam. Cu K α radiation was used (40 mA, 40 kV) and the spectra was obtained in the range 3°–30° 2 θ .

2.10. Fourier Transform-Infrared spectra (FT-IR)

Studies of FT-IR spectroscopy were conducted with an IR spectrophotometer (Jasco FT-IR A-200, Milan, Italy) using the KBr disc method. The samples were mixed with KBr and compressed into a tablet (10 mm in diameter and 1 mm in thickness) using a manual hydraulic tablet

presser (Perkin Elmer, Norwalk, CT, USA) at 4000 kg/cm for 4–6 min.

2.11. Water uptake studies

Sample (10–15 mg) of freshly prepared SDs were accurately weighted in DSC pans without lid and moved to a 25 °C, 85 % RH chamber. At determined time points, sample weight was recorded to calculate the water level.

3. Results and discussion

3.1. KET solubility/miscibility with semicrystalline carriers

3.1.1. Melting point depression study by thermal analysis

The miscibility of KET with the three semicrystalline carriers was studied via the melting point depression (MPD) approach using DSC. This approach has been widely used to determine the drug-polymer miscibility for polymers, including semicrystalline ones (Marsac et al., 2008, 2006).

Fig. 2A represents the DSC thermograms for pure KET and its PM with the three carriers at different weight fractions (from 100 % KET to 75 % KET at 5 % decrements). Pure KET has a melting point at 94.18 °C ($T_{m,Onset} = 92.37$ °C and $T_{m,End} = 95.15$ °C). There is a clear evidence of the depression of the melting point of KET in the mixtures: as the carrier amount in the PMs increased, the onset temperature as well as the heat of fusion is gradually reduced. The extent of MPD observed increasing the carrier to drug ratio can be used to evaluate the miscibility of a specific binary system (Forster et al., 2001). If the drug is miscible with the carrier, the Gibbs free energy of the mixture will be lower than that of the two components alone. As the chemical potential of the drug will be lowered through mixing with the polymer, the melting point will be

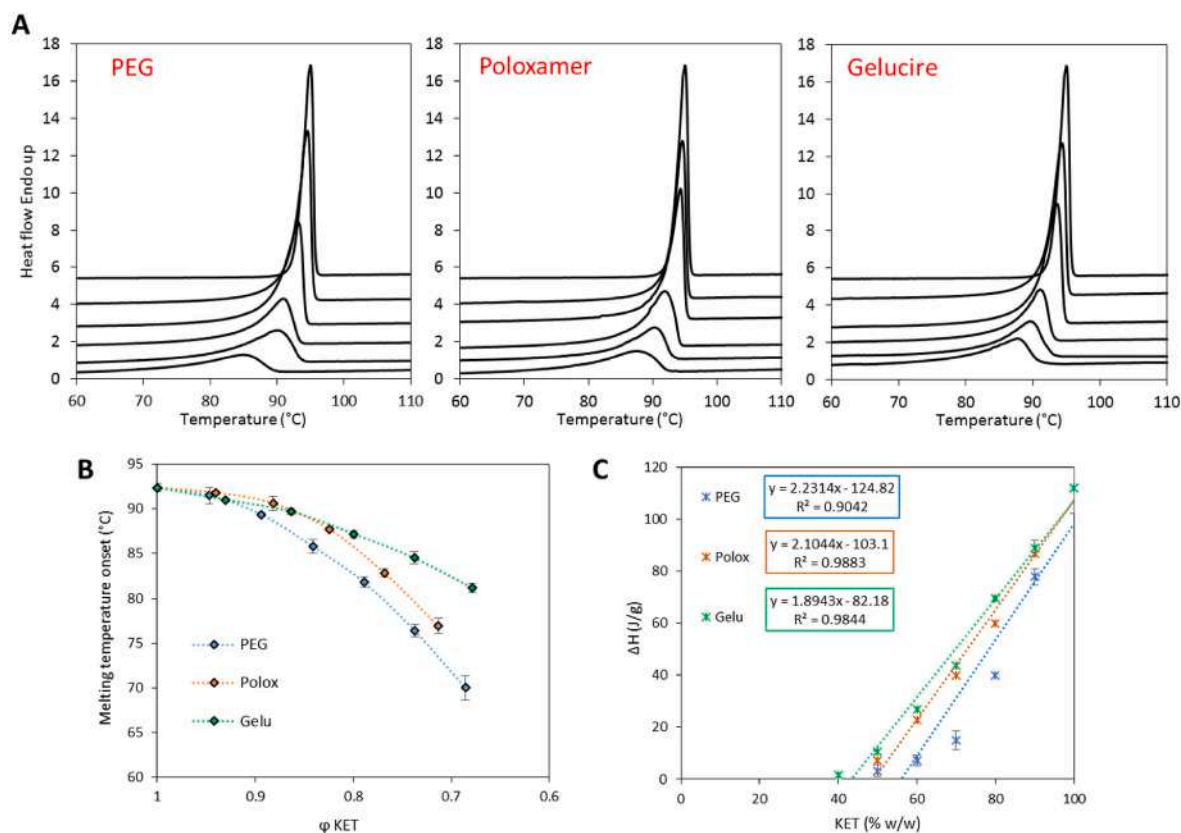


Fig. 2. DSC thermograms with PM of KET and 0, 5, 10, 15, 20 and 25 % w/w (from the top to the bottom) of the different carriers measured at a heating rate of 1 °C/min (A). T_{onset} of the melting endotherm for KET mixtures with the different carriers as a function of volume fraction of KET (B). Enthalpy of melting for KET with the different carriers as a function of KET weight fraction and the relative linear regression analysis (C).

depressed as well. Therefore, the significant MPD observed for KET upon addition of the semicrystalline carriers indicates a significant degree of mixing at the drug melting temperature.

The extent of MPD for the three drug-carriers mixtures can be evaluated by plotting the the $T_{m, \text{onset}}$ of KET melting endotherm for the various mixtures as a function of volume fraction of KET (Fig. 2B). Clearly, PEG reduced the melting temperature to a larger extent than the other two carriers, while Gelucire caused the lowest MDP.

Fig. 2C shows the enthalpy of melting of KET for the various KET-carrier mixtures. The enthalpy of melting (ΔH_m) of pure KET is 112.03 ± 1.46 J/g. By plotting the melting enthalpies versus KET fraction, a linear relationship is observed with good correlation coefficients ($R^2 > 0.9$). Extrapolation of the linear data for the reduced melting enthalpy to zero enthalpy can be used to predict the KET-carrier weight fraction at which no drug melting can be detected (melting endotherm equal to 0 J/g) (Altamimi and Neau, 2018; Amharar et al., 2014). The zero enthalpy of melting for KET occurs at 55.94, 48.99, and 43.38 % w/w in PEG, Poloxamer, and Gelucire, respectively, as shown in Table 2 and discussed below.

3.1.2. Flory-Huggins interaction parameter (χ) and Gibbs free energy of mixing

Further insights into KET-carrier miscibility were obtained by calculation of the FH interaction parameter. The extent of melting point depression of a specific drug-polymer system can be related to the drug-polymer interaction parameter, χ , an indicator of drug-polymer miscibility according to Flory-Huggins theory, and χ can be further used to determine the Gibbs free energy of mixing (Marsac et al., 2006).

For PEG, Poloxamer and Gelucire-based binary mixtures with KET, interaction parameters with a value of -5.23 ($R^2 = 0.999$), -4.42 ($R^2 = 0.991$) and -1.70 ($R^2 = 0.998$) were obtained, respectively (Fig. 3A). The negative values of χ for all three systems indicate that all carriers were miscible with the API at the temperature near the melting temperature of the drug and suggest the presence of adhesive interaction between drug and carrier molecules. This means that drug-carrier interactions are preferred over drug-drug and polymer-polymer interactions. Moreover, the FH theory suggests a rank order, from the greatest interactions to the least, PEG > Poloxamer > Gelucire.

FH interaction parameter values were used to calculate Gibb's free energy of mixing (ΔG_{mix}) using Eq. (2). Fig. 3B, C and D show the free energy of mixing of KET-PEG, KET-Polox and KET-Gelu systems as a function of drug volume fraction, including the entropic and enthalpic contributions, across the range of the volume fraction of each carrier. The ΔG_{mix} for a specific drug-carrier composition can be either positive (indicating unfavorable mixing) or negative (indicating spontaneous mixing). Considering the three terms of Eq. (2), the first two terms describe the entropic contribution while the last term represents the enthalpic contribution to the total free energy of mixing of the binary system. As the mixing cause disorder and hence reduce entropy, the total entropic contribution is expected to always favorite mixing. Differently, the enthalpic contribution depends on the adhesive and cohesive interactions which are reflected on the interaction parameter χ . Therefore, the enthalpic component is going to determine whether $\Delta G_{\text{mix}} \leq 0$ or not (Thakral and Thakral, 2013).

The $\Delta G_{\text{mix}}/RT$ curves for the three drug-carrier investigated were

Table 2

Solubility values of KET (% w/w) in three semicrystalline carriers evaluated with three different methods.

Carrier	KET solubility (% w/w)		
	Zero enthalpy extrapolation	MDP curve (70 °C, T_{peak})	Experimental (70 °C)
PEG	55.94	57.5	51.50 ± 0.96
Poloxamer	48.99	51.9	47.04 ± 0.03
Gelucire	43.38	49.4	44.14 ± 0.37

concave up and show negative values for all mixtures. This result predicts spontaneous mixing of KET with each carrier, as the interaction parameters were negative, $\chi \leq 0$.

3.1.3. Construction of the phase diagram

In order to provide an estimation of the saturation limit of KET loading in the carriers at different temperatures, temperature-composition phase diagrams were constructed (Fig. 4) using DSC thermal data: the melting temperature of the carrier in the mixture (dashed grey line) and the melting point curve of the API in the mixture (colored lines). The experimental (solid curves) and the predicted (dashed curves) KET melting points were plotted by considering either T_{onset} (blue curves), T_{peak} (orange curve) or T_{end} (red curves) values. Phase diagrams confirmed that the presence of the polymer causes the depression of the melting point of KET. Conversely, the presence of KET did not significantly impact the carrier melting point. The MPD curve, or liquidus line, represents the solubility of the drug in the carrier as a function of temperature under equilibrium conditions, and the region above it consists in one phase liquid system (Law et al., 2002). The extrapolation of this curve to lower temperatures allows to predict the exact intersection point with the melting temperature of the mixture: the correspondent drug-carrier fraction can be considered the maximum amount of API that can solubilize in the carrier (Prudic et al., 2014; Tian et al., 2013). Comparing the three KET-carrier systems, it is immediately evident that the solubility curve of KET in Gelucire shifted toward lower composition range, indicating a limited solubility of KET in this carrier.

The temperature-composition phase diagram has a practical utility for the selection of process parameters (e.g. working temperature) and formulation parameters (e.g. type of carrier and drug loading) for the manufacturing of SDs (Moseson and Taylor, 2018). The solubility curves give an indication about KET solubility/miscibility with the carrier at a specific temperature. Selecting a processing temperature lower than the liquidus line for a given composition would achieve a one-phase system where drug crystals can fully dissolve in the polymer. In the present study, for example, phase diagrams showed that a working temperature of 70 °C could be suitable for production of SDs with drug loadings below 40 % w/w of KET.

Table 2 summarizes the predicted solubility values of KET in the three semicrystalline carriers at 70 °C and compare them to the values obtained experimentally, which are reported in Figure S1. KET dissolves in molten carriers to a large extent (from 44 % to 51 % w/w of drug dissolved), confirming a favorable drug miscibility with the three semicrystalline carries. The rank of order was: PEG > Poloxamer > Gelucire, consistent with the FH-based interaction parameter data. The solubility values extrapolated from the melting enthalpy data to zero enthalpy were very similar to the solubility results obtained experimentally, with differences always below 5 % w/w for all three carriers. Regarding the predicted solubility values calculated from MDP method based on thermal data, the curve based on T_{peak} values better fitted the experimental data compared to the curves constructed on T_{onset} and T_{end} , and was only slightly overestimated relative to experimental solubility values.

3.2. Characterization of KET-carrier SDs

3.2.1. Microstructure of SDs

Fig. 5 shows the PLM images of SDs with different compositions. Pure carriers crystallized very fast at ambient conditions and showed a characteristic morphology consisting of multiple spherulites. Each spherulite contains a large number of lamellar crystallites, radiating in all directions from a central nucleus with molecular chains oriented tangentially (Zhang et al., 2018). Under polarized light, this arrangement formed a set of four symmetrically disposed sectors for each spherulite, called Maltese cross.

Pure PEG showed well-defined morphology with spherulites with diameters up to 1 mm. All SDs of KET and PEG were crystalline, but

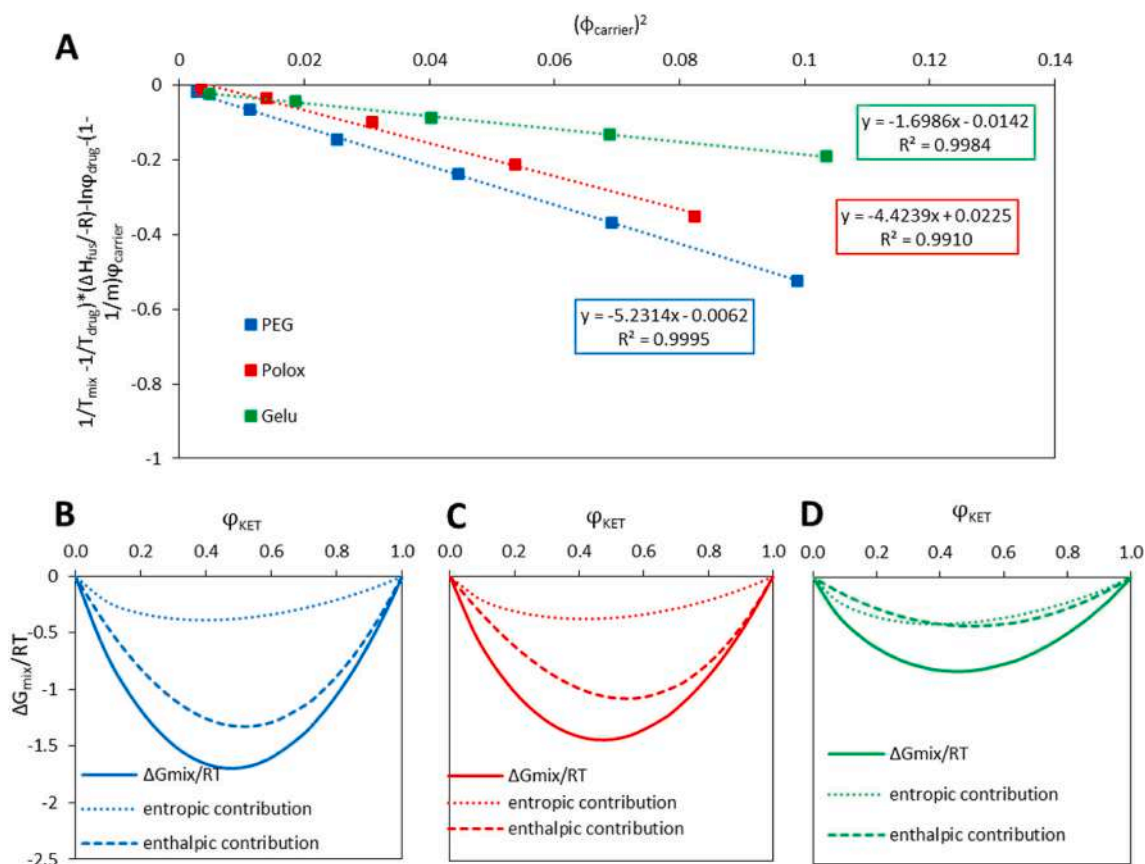


Fig. 3. Plot used to calculate the Flory-Huggins interaction parameter for KET-PEG, KET-Polox and KET-Gelu systems according to Eq. (1), the slope represented the value of the FH interaction parameter (A). Temperature-normalized Gibbs free energy ($\Delta G_{\text{mix}}/RT$) versus drug volume fraction (ϕ) for KET and PEG (B), Polox (C) and Gelu (D).

increasing the drug amount, Maltese cross becomes less defined. Specifically, when KET amount was higher than 30 %, spherulites lose their symmetry and two or three sectors of high birefringence were observed. With increasing drug amount, the spherulites tended also to increase in size, probably as consequence of differences in the crystallization process (e.g. higher distance amongst nucleation sites). However, in all PEG-based SDs the spherulites were space-filling with no evidence of KET accumulation in the interspherulitic space.

Pure Poloxamer gave a well-defined pattern with spherulites ranging from about 200 to 600 μm , separated from one another by sharp interfaces. The addition of KET led to morphological changes similar to those observed for PEG, i.e. larger spherulites and less defined Maltese cross. In case of Poloxamer, however, fibrils with a different contrast radiate from the center of the spherulite and at 30 % of KET the four sectors of high birefringence typical of Maltese crosses completely disappeared. At 40 % of drug, an amorphous region, appearing as dark, was observed between adjacent spherulites while crystallization took place.

As a mixture of glycerides, PEG esters of fatty acids and pure PEG, Gelucire exhibit a complex morphology and its crystalline patterns showed large spherulites with a tessellated structure consisting of small birefringent fibrils. In this case, the addition of KET led to the disappearance of the spherulites, although the tessellated crystalline pattern can be observed with 10 and 20 % of KET. With further increase in drug amount, the SDs are characterized by dark amorphous areas as well as crystalline branched structures with weak birefringence growing within. Similar morphologies have been previously observed for ultrathin films of PEO/PMMA blends (Ogieglo et al., 2014) or PCL (Mareau and Prud'homme, 2005) and have been defined as "fractal seaweed" and "fractal dendrite" (Yu et al., 2017). Thus, KET-Gelu systems with at least 30 % w/w of drug were only partially crystalline with crystals showing a

different morphology compared to the pure carrier.

3.2.2. Thermal behaviour and solid state characterization of SDs

First, DSC of KET-carrier SDs were performed at a scanning rate of 10 $^{\circ}\text{C}/\text{min}$ and compared with those of raw carriers and pure carriers subjected to melt-cooling (Fig. 6). For all three systems, the melting behaviour of the carrier significantly changed in the SDs with KET. Specifically, the carrier $T_{\text{m, onset}}$ and its enthalpy of fusion decreased as a function of KET amount in the SD, showing that the presence of KET influenced the carrier solid state. The dilution effect (lower carrier amount in the SDs at increasing drug loading) could explain the decreased melting enthalpy. Otherwise, the low enthalpy of fusion might indicate decreased crystallinity or a delayed crystallization time compared to pure carriers. With 40 % of KET, the melting peak of PEG and Gelucire were almost absent, suggesting that freshly produced SDs were mostly amorphous, consistently with PLM observation. Moreover, a small endothermic event at about 58 $^{\circ}\text{C}$ was observed in all Gelucire-based SDs. Thus, PXRD was used to investigate the nature of Gelucire-based SDs. Fig. 7A showed the diffractograms of SDs with low (10 %) and high (40 %) KET amount and their corresponding PMs. The SD with 10 % of KET showed only the carrier diffraction peaks, indicating a crystalline system with no sign of crystalline drug (which was detected in the corresponding PM). The freshly prepared SDs with 40 % KET and 60 % Gelucire had semisolid consistency (Fig. 7B) and its diffractogram indicated a completely amorphous system with no diffraction peaks (Fig. 7A), consistently with the morphological observations by PLM (Fig. 5) and DSC curves (Fig. 6). After 7 days, the sample showed partial crystallization (Fig. 7B). Hence, these results confirmed the hypothesis of increased crystallization time for Gelucire-KET systems; KET acted as crystallization inhibitors for Gelucire and at high drug amount the

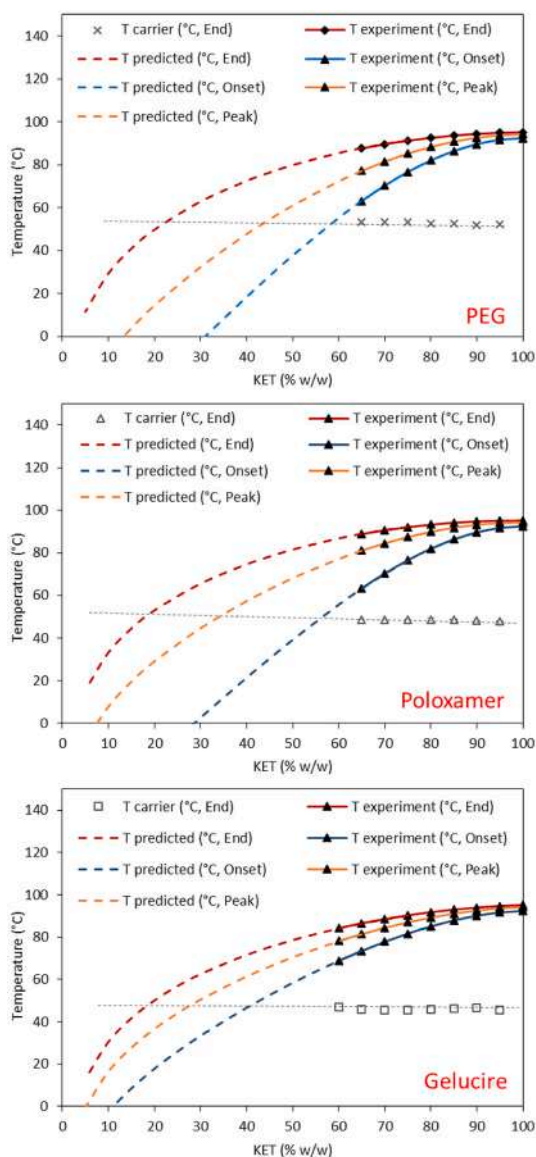


Fig. 4. Phase diagrams of KET mixtures with PEG, Poloxamer and Gelucire: the solid curves represent the melting point depression experimental data, while the dashed curves extrapolate the data to lower temperatures basing on Eq. (2) using either T_{onset} (blue curves) or T_{end} (red curves). Solubility curves intersect melting curves of the carrier in the mixture based on the carrier T_{end} . (For interpretation of the references to colour in this figure legend, the reader is referred to the web version of this article.)

crystallization of the carrier was completely prevented.

It is also of interest to consider the influence of the APIs on the crystallization of the carrier; thus, molten KET-carrier samples were cooled at 2 °C/min and then slowly reheated at 1 °C/min to verify the physical form crystallized upon.

The crystallization of pure carriers observed during cooling was recorded as a single broad exothermic peak with onset temperatures ($T_{\text{cr, onset}}$) of 45.07 and 41.15 °C for PEG and Polox, respectively (Fig. 8A and 8B). The main crystallization exotherm was not detected for both Gelucire and its SDs, as for this carrier crystallization was more slowly.

In case of SDs with PEG, the $T_{\text{cr, onset}}$ of carriers was decreased to varying extent with KET addition (Fig. 8A). This can be seen as a crystallization inhibition effect due to incorporation of the drug into the carrier matrix. However, the effect on crystallization should not be evaluated on the T_{cr} as an absolute value, but rather considering the supercooling degree of the system, namely the difference between

melting and crystallization temperature which represents the driving force for nucleation and crystal growth from the melt. It should be considered that mixing of KET with PEG decreased the melting temperature of the binary system by few degrees (about 2–3 °C every 10 % KET added). From our DSC results, the supercooling degree of pure PEG was 20.2 °C, in accordance with previous studies (Paberit et al., 2020). Taking into account the melting point depression effect upon KET mixing, the degree of supercooling of KET-PEG systems was calculated to be around 20 °C, thus meaning that the driving force for the phase transformation was equal between SDs and pure carriers. The same calculations were made for Polox, where the supercooling degree was 15.6 °C for the pure carrier and ~ 17 °C for SDs, again indicating a negligible effect of KET on crystallization behavior.

After crystallization, the samples were reheated at 1 °C/min. For Polox, only one endothermic event was detected (data not shown), showing the melting of the SD in a single event as already seen by DSC scan at 10 °C/min (Fig. 6B). Differently, thermograms of PEG systems (Fig. 8C) showed two distinct endothermic events, the first at about 56 °C and the second at 61 °C for pure PEG, which moved to lower values with increasing KET amount. This behavior is related to the crystallization of PEG either in extended chains or in folded chains (Chen et al., 2015; Paberit et al., 2020; Van Duong et al., 2018). Whereas the former is the more stable molecular arrangement, thus corresponding to the higher T_m , the latter is metastable as the one-time folded PEG chains tend to convert into a more stable arrangement overtime by unfolding (Ginés et al., 1996). These two types of “crystals” formed at the same time during crystallization (Fig. 8A) but had a different melting point. This was further confirmed by observation under Hot-stage PLM of the KET:PEG 20:80 SD (Fig. 8D). The microstructure of PEG crystals changed at 51 °C as a consequence of the melting of the folded-chain crystalline fraction, followed by a rearrangement of the remaining PEG crystals, which finally melted at 58 °C. It should be also noted that the higher T_m crystals were already present in the sample and did not formed during heating, corroborating the fact that the original sample consisted in both type of crystals.

The enthalpy (ΔH_m) values of the melting peaks from the folded and non-folded crystals of PEG, expressed as % of the total enthalpy of both endotherms, were calculated and are shown in Fig. 8E. In pure PEG, directly after crystallization, the extended-chain form was predominant (~73 %), while a linear decrease of the intensity related to this crystal form was observed with the addition of KET. The tendency of small molecules in promoting PEG crystallization in the folded form rather than the non-folded one has been previously observed for small lipids (Unga et al., 2010) and suggested the incorporation of KET into the amorphous regions of the polymer crystallites (interlamellar or interfibrillar regions).

Finally, the total crystallinity was calculated by the enthalpy of the melting peak (or the sum of both melting peaks in case of PEG) taking 198 J/g and 139 J/g as the ΔH_m of 100 % crystalline PEG and Polox, respectively (from the first heating of pure carriers). The calculated crystallinity was then normalized by the weight fraction of carrier in the SDs to obtain the crystallinity per gram of carrier. The % crystallinity was seen to be constant in all PEG SDs, with values ranging from 90 to 95 % PEG crystallinity. For Polox, the % of crystallinity in the SDs was 95 %, compared to 90 % of pure carrier. Thus, no significant and concentration-dependent effect of KET on carrier crystallinity was observed.

Overall, the characterization of SDs indicate that upon mixing of KET up to 40 % w/w with different semicrystalline carriers, no crystal of pure KET was observed, suggesting the incorporation of drug molecules in a (mostly) crystalline system. KET, therefore, once dissolved in the molten carrier, remains molecularly dispersed even while polymers re-crystallizes during cooling to room temperature. As for PEG and Polox, it is known that drug molecules can be incorporated in different location of the semicrystalline matrix (Zhu et al., 2010). As PLM analysis did not show any evidence of interspherulitic accumulation for any of

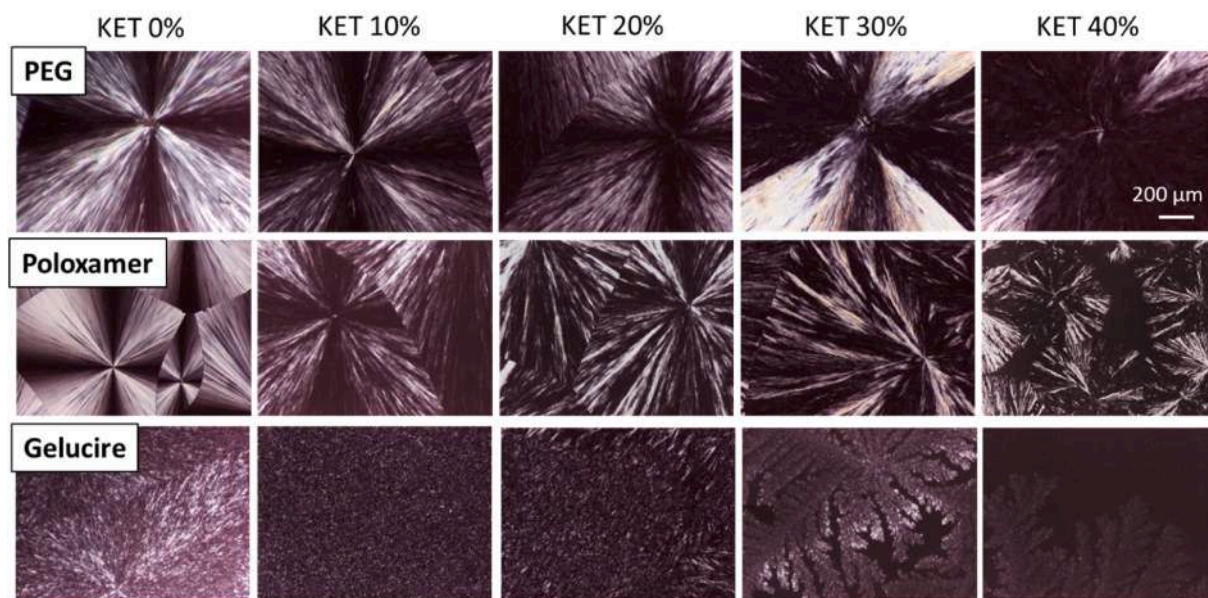


Fig. 5. Polarized optical microscopy images of pure carriers and KET-carrier SDs (from 10 to 40% w/w KET) analysed immediately after cooling.

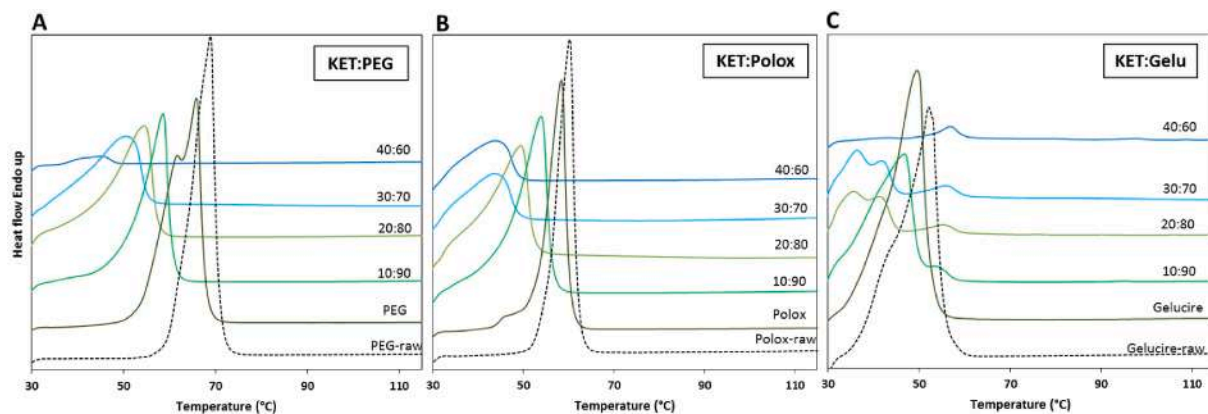


Fig. 6. DSC heating curves of pure carriers as raw materials, pure carriers after being subjected to melt-cooling and freshly prepared KET-carrier SDs (from 10 to 40% w/w KET) with PEG (A), Polox (B) and Gelu (C).

the three systems studied, we can hypothesized that KET molecules were included into the interlamellar or interfibrillar regions.

3.2.3. KET-carrier interactions in SDs

The drug molecules may interact with the polymer molecules via several weak forces (e.g. H-bonding, van der Waals forces, ionic, hydrophobic) at the solid state and different authors described the role of these intermolecular bonds in stabilizing SD systems (Paudel et al., 2013). Thus, molecular interactions between semicrystalline carriers and KET was investigated using FT-IR (Fig. 9).

Crystalline KET was characterized by two carbonyl signals at 1697 and 1655 cm^{-1} , corresponding to the dimer hydrogen bonded C=O of the carboxylic acid and the C=O of the ketone, respectively (Vueba et al., 2006). In the amorphous form, these stretching vibrations were moved to 1707 cm^{-1} (with a shoulder at 1735 cm^{-1}) and to 1659 cm^{-1} , respectively. Moreover, the peak shoulder at 1735 cm^{-1} can be assigned to the free acid carbonyl group (Browne et al., 2020; Gupta et al., 2003). In the fingerprint region, crystalline KET showed three distinct peaks at 717, 703 and 691 cm^{-1} , while only two peaks are present when the drug is amorphous (Vueba et al., 2006). Therefore, these differences can be used as indicators of the physical state of the drug in the samples.

In all SD samples, two bands relative to C—H out-of-plane bending at

722 and 703 cm^{-1} were clear indications of amorphous KET, while the corresponding PMs showed the three bands of crystalline drug at 717, 703 and 691 cm^{-1} . In the carbonyl region, of all SDs spectra showed an intense band at $\sim 1731 \text{ cm}^{-1}$, which was broader and shifted with respect to the signal of both pure KET (at 1697 cm^{-1}) and PMs (at 1697–1698 cm^{-1}). The result suggested that the carbonyl group of the carboxylic acid was involved in intermolecular interactions with the carriers. Differently, the band at 1655 cm^{-1} relative to ketone C=O stretching was unchanged. Moreover, the broad band of the O—H stretching of carboxylic acid observed in the PM samples at about 3465 cm^{-1} was shifted down to 3450 cm^{-1} . Therefore, the interactions seemed to involve the OH and C=O moieties of the carboxylic acid group of KET, rather than the ketone C=O.

Finally, by comparing the three carriers it should be noted that the additional band indicative of drug-carrier hydrogen bond formation was seen at 1730 cm^{-1} when the carrier was PEG, but the red-shift was even higher in case of Polox and Gelu (1732 cm^{-1}), suggesting that a stronger H-bond was formed. Moreover, for Polox and Gelu, a less intense band at $\sim 1730 \text{ cm}^{-1}$ was detected also in PMs, which was absent in case of PEG.

The FT-IR analysis of the KET-Gelu PMs and SDs with different composition ratios (Figure S2) allowed to evaluate the role of drug

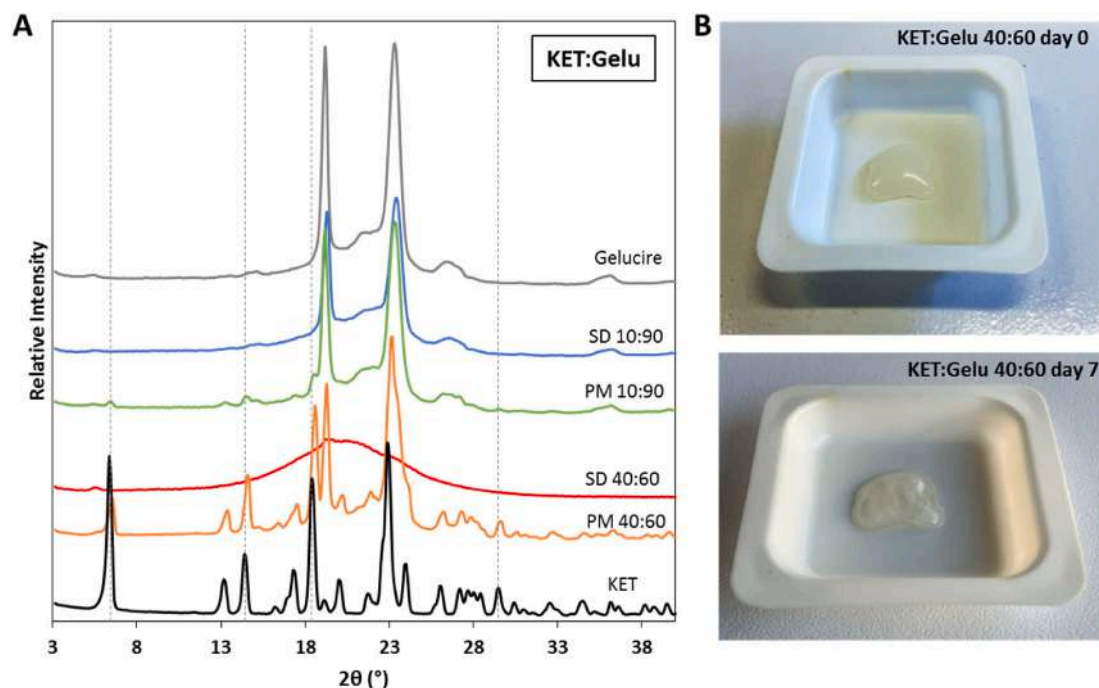


Fig. 7. PXRD pattern of raw Gelucire, raw KET, Gelucire-based SDs with 10 % and 40 % KET and their corresponding PMs (A). Appearance of KET:Gelu 40:60 immediately after production and after 7 days (B).

amount on drug-carrier interactions. The presence of the broad band at $\sim 1731\text{ cm}^{-1}$ for all SDs confirmed that the formation of KET-Gelu hydrogen bonds takes place with all drug amounts. Nevertheless, it was interesting to observe differences in the case of the PMs: as evidenced from the blue region, passing from PMs with high drug amounts to PMs with low drug amounts, the band at 1697 cm^{-1} (C=O of the carboxylic acid of KET non hydrogen bonded) gradually decreased its intensity, together with the increased intensity of the band at 1731 cm^{-1} (C=O of the carboxylic acid of KET hydrogen bonded with the carriers hydroxyl groups). This suggests that the increasing of the carrier amount in the mixture facilitates the establishment of the drug-carrier interactions, even in the simple powder mixture where KET was crystalline.

Thus, from FT-IR investigations it can be concluded that:

- (i) KET is in the amorphous form in the SDs;
- (ii) The carboxylic acid group of KET is involved in hydrogen bonds with the hydroxyl groups of the three carriers;
- (iii) KET interaction with Polox and Gelu seem stronger than KET interaction with PEG.

3.2.4. Physical stability of SDs

Aging and phase separation are commonly observed in SDs during storage, possibly leading to separation of the drug from the carrier. This process starts with separation of amorphous drug from the SD matrix, drug molecules migration and generally continues with drug recrystallization (Zhang et al., 2021). To assess the stability of SDs, the physical state of SDs were monitored after 6 months of storage at $25\text{ }^{\circ}\text{C}$ and 30 % RH. PLM images, reported in Fig. 10 showed KET crystals in PEG-based systems with drug loading $\geq 20\%$ KET as well as in Polox-based SDs with 40 % of KET. PXRD data confirmed these observations (Figure S3 and S4). As for Gelu-based SDs, observation under PLM did not show clear drug crystallization, however PXRD (Figure S5) revealed diffraction peaks of both the carrier and the drug in the SD with 40 %w/w of KET.

Therefore, drug crystallization at 40 % w/w of KET was observed for all SDs despite values of χ and ΔG_{mix} calculated using FH theory were

negative (Fig. 3), indicating that KET have an exothermic spontaneous mixing with the three carriers (Bansal et al., 2016).

The physical stability of SDs depends on both thermodynamic and kinetic factors (Lin et al., 2018). We should consider that the FH theory, used to evaluate the thermodynamic aspects of the SDs, involves a number of simplifying assumptions which are not fully appropriate for some drug-carrier systems (Meere et al., 2019). For instance, the thermodynamics of systems involving drug-carrier interactions can partially deviate FH model. This is the case of the present SDs, where KET has been proven to form strong intermolecular hydrogen bonds with the carriers, specifically Polox and Gelu. Indeed, hydrogen-bonded systems violate the key assumptions at the basis of regular solution theories (Anderson, 2018) and the model does not consider the variations of types and strengths of drug-polymer interactions at varying external parameters (e.g. temperature). For instance, the lower extent of hydrogen bonding between PEG and the carboxyl moiety of KET compared to the other two carriers may be one of the possible reasons accounting for the lower physical stability of KET-PEG SDs.

Moreover, phase separation and drug recrystallization in SDs are closely related to the drug molecular mobility. KET has low T_g ($\sim -3^{\circ}\text{C}$), therefore, mobility is expected to be high at the process ($70\text{ }^{\circ}\text{C}$) and storage temperature ($25\text{ }^{\circ}\text{C}$). As a consequence, drug diffusion from the interlamellar/interfibrillar polymer regions in case of crystalline SDs is expected and it may increase with temperature and humidity during storage (Zhang et al., 2021). Specifically, even small amounts of moisture in the SD might significantly affect the mobility of the drug and thus drug migration and recrystallization (Lin et al., 2018). Thus, the water uptake of pure carriers and SDs with 40 % of KET were evaluated and the results are shown in Fig. 11. Pure carriers were observed to absorb moisture, in particular PEG and Poloxamer were extremely hygroscopic and characterized by deliquescence behavior, in accordance to literature data (Baird et al., 2010a; Wu et al., 2017). Due to the hydrophobicity of KET, the water uptake curve of SDs containing 40 % w/w of drug were significantly reduced with respect to pure carriers, although the extent of moisture sorption was maintained for the three carriers in the order $\text{PEG} > \text{Polox} > \text{Gelu}$. Thus, the higher extent of moisture adsorption of PEG-based SDs when stored at humid conditions can (at least partially)

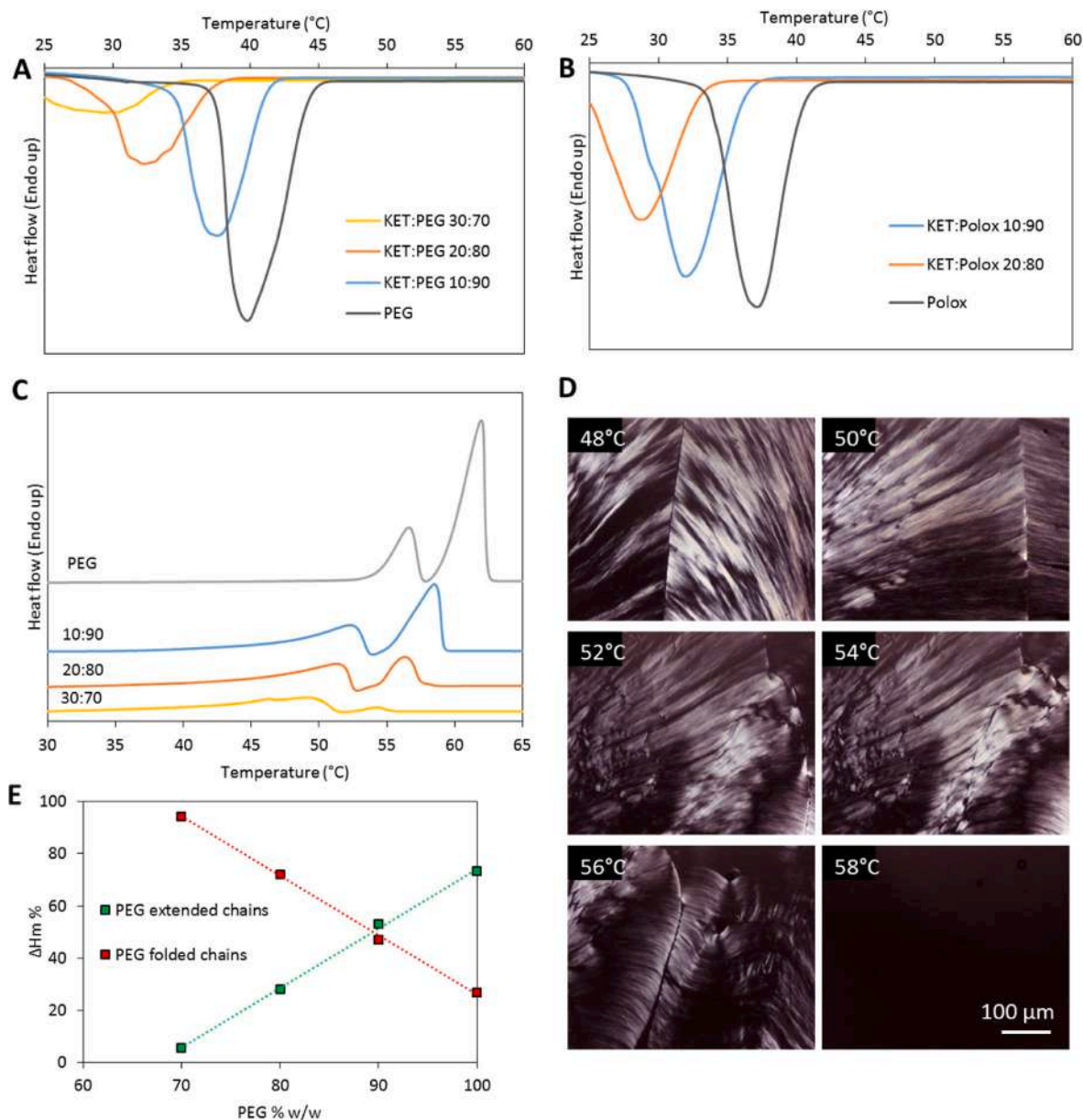


Fig. 8. DSC cooling curves at 2 °C/min of KET:PEG (A) and KET:Polox (B) systems showing SDs crystallization exotherm. DSC heating curves at 1 °C/min of KET:PEG systems following crystallization (C). Hot-stage polarized optical microscopy images of KET:PEG 20:80 system during heating at 1 °C/min (D). Percentage ratio of the melting enthalpy (ΔH_m %) of the extended-chain and to the folded-chain crystalline forms of PEG at varying KET amount (E).

account for the lower stability of KET-PEG SDs. Conversely, the lower water uptake of Gelu-based systems, which is related to the partially lipophilic composition of this carrier (a fraction of mono, di and triglycerides of Gelucire®50/13), can contribute to SDs stability.

Finally, the carrier crystalline structure might have an influence on the SDs stability: in case PEG, where experimental data suggested drug incorporation into the amorphous polymer regions, the secondary crystallization process of PEG when unfolding of lamellae occurs, could contribute to drug migration out of the interlamellar/interfibrillar domains and favor phase separation.

4. Conclusion

In this work, three semicrystalline materials (PEG, Poloxamer and Gelucire) were evaluated as carriers for the preparation of KET-loaded SDs, as an alternative formulation to conventional ASD based on

amorphous polymers. As the selected drug was highly miscible with all carriers (maximum solubility ranging 44–51 % w/w at 70 °C), KET directly dissolved into the molten carriers and SDs up to 40 % w/w of KET were prepared with melting-based process at a temperature below the drug melting point. From DSC, PLM and PXRD data of PEG and Poloxamer-based SDs, it could be observed that the polymers solidified in the semicrystalline state, while the drug became amorphous. In particular, the preferential crystallization of PEG in folded-chain form and the change in the SDs microstructure suggested the incorporation of KET in the amorphous (interlamellar or interfibrillar) regions of the solid polymer. Differently, KET retarded the crystallization of Gelucire and high drug loadings led to amorphous and semisolid systems. Stability studies after 6 months of storage evidenced phase separation in PEG-based SDs even at 20 % KET loading, while Poloxamer and Gelucire-based SDs showed KET crystallization only at 40 % KET.

Concluding, this study allowed to understand the different

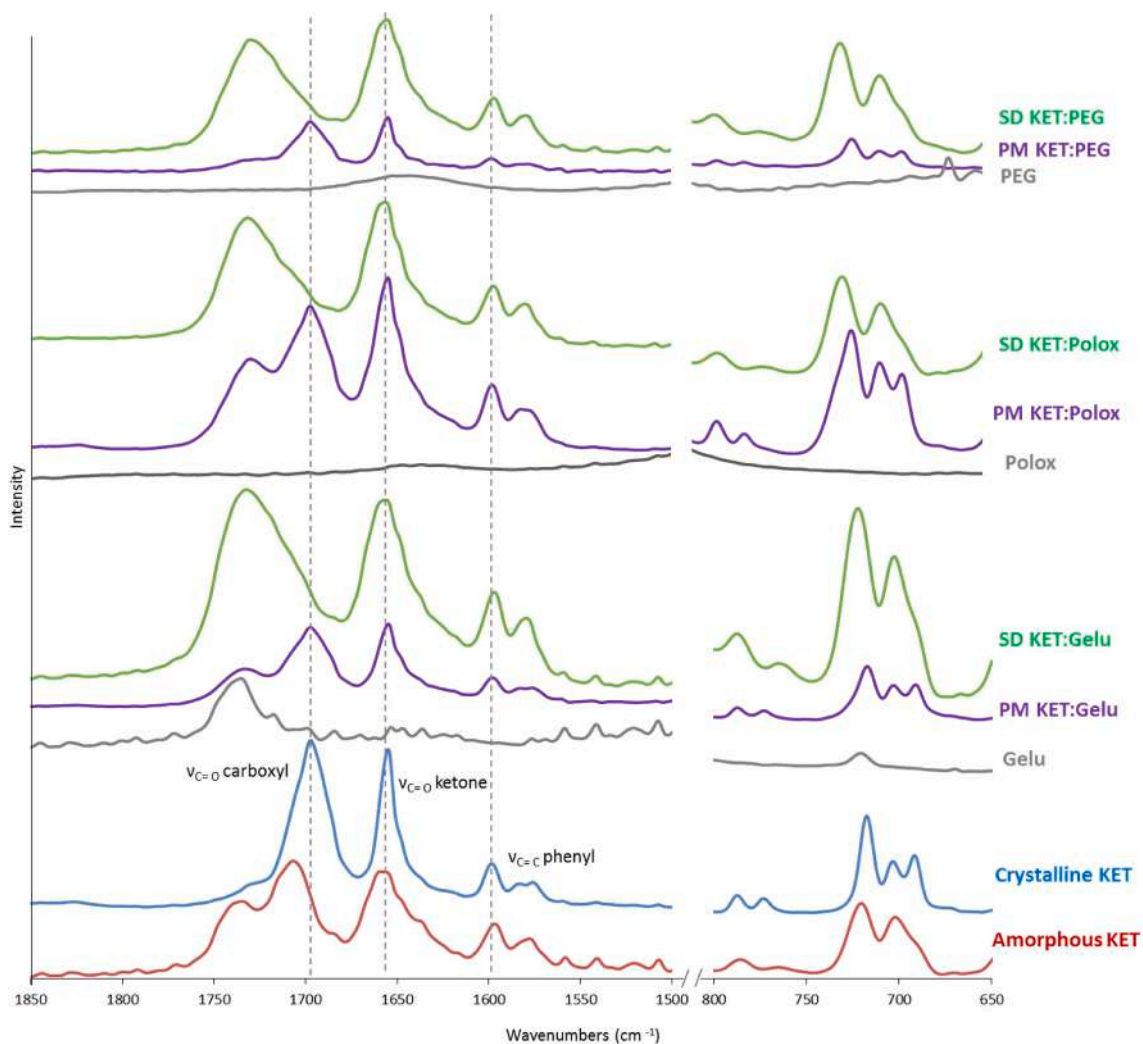


Fig. 9. FT-IR spectra of pure KET (crystalline and amorphous), SDs with 40% KET with all three carriers and their corresponding PMs.

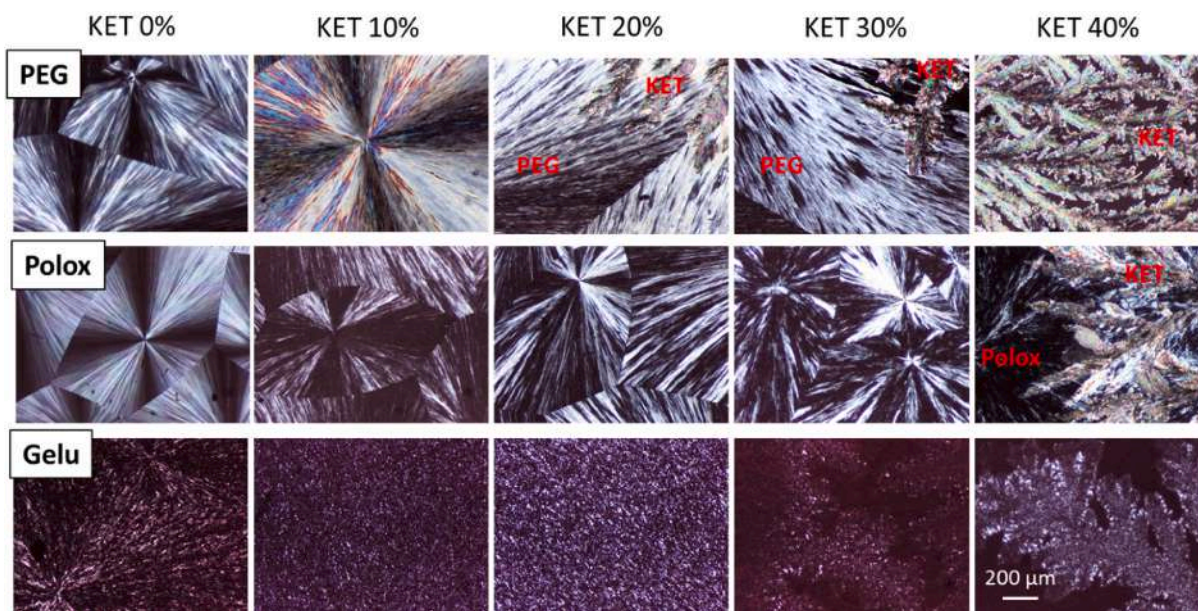


Fig. 10. Polarized optical microscopy images of pure carriers and KET-carrier SDs (from 10 to 40 % w/w KET) analysed after 6 months of storage at 25 °C and 30 % RH.

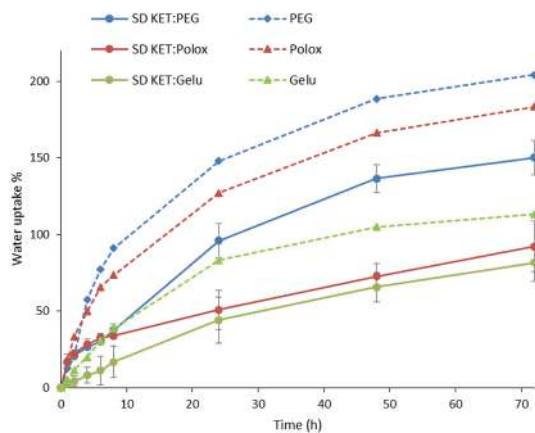


Fig. 11. Water uptake of pure carriers after being subjected to melt-cooling and freshly prepared KET-carrier SDs (40 % w/w KET) plotted against storage time at 25 °C, 85 % RH.

physicochemical properties, including phase behavior, drug-carrier interactions and physical stability, of SDs prepared with low-melting semicrystalline carriers, and how the different semicrystalline excipients contribute to these properties, providing information for the design and improvement of the final formulations.

CRedit authorship contribution statement

Serena Bertoni: Conceptualization, Formal analysis, Investigation, Writing – original draft. **Beatrice Albertini:** Conceptualization, Validation, Writing – review & editing, Supervision. **Nadia Passerini:** Conceptualization, Resources, Writing – review & editing, Supervision.

Declaration of Competing Interest

The authors declare that they have no known competing financial interests or personal relationships that could have appeared to influence the work reported in this paper.

Data availability

Data will be made available on request.

References

- Abdelkader, H., Abdallah, O.Y., Salem, H., Alani, A.W.G., Alany, R.G., 2014. Eutectic, monotectic and immiscibility systems of nimesulide with water-soluble carriers: phase equilibria, solid-state characterisation and in-vivo/pharmacodynamic evaluation. *J. Pharm. Pharmacol.* 66, 1439–1450. <https://doi.org/10.1111/jphp.12277>.
- Alshehri, S., Imam, S.S., Hussain, A., Altamimi, M.A., Alruwaili, N.K., Alotaibi, F., Alanazi, A., Shakeel, F., 2020. Potential of solid dispersions to enhance solubility, bioavailability, and therapeutic efficacy of poorly water-soluble drugs: newer formulation techniques, current marketed scenario and patents. *Drug Deliv.* 27, 1625–1643. <https://doi.org/10.1080/10717544.2020.1846638>.
- Altamimi, M.A., Neau, S.H., 2016. Use of the Flory-Huggins theory to predict the solubility of nifedipine and sulfamethoxazole in the triblock, graft copolymer Soluplus. *Drug Dev. Ind. Pharm.* 42, 446–455. <https://doi.org/10.3109/03639045.2015.1075033>.
- Altamimi, M.A., Neau, S.H., 2018. A study to identify the contribution of Soluplus® component homopolymers to the solubilization of nifedipine and sulfamethoxazole using the melting point depression method. *Powder Technol.* 338, 576–585. <https://doi.org/10.1016/j.powtec.2018.07.027>.
- Amharar, Y., Curtin, V., Gallagher, K.H., Healy, A.M., 2014. Solubility of crystalline organic compounds in high and low molecular weight amorphous matrices above and below the glass transition by zero enthalpy extrapolation. *Int. J. Pharm.* 472, 241–247. <https://doi.org/10.1016/j.ijpharm.2014.06.038>.
- Anderson, B.D., 2018. Predicting Solubility/Miscibility in Amorphous Dispersions: It Is Time to Move Beyond Regular Solution Theories. *J. Pharm. Sci.* 107, 24–33. <https://doi.org/10.1016/j.xphs.2017.09.030>.

- Baird, J.A., Olayo-Valles, R., Rinaldi, C., Taylor, L.S., 2010a. Effect of Molecular Weight, Temperature, and Additives on the Moisture Sorption Properties of Polyethylene Glycol. *J. Pharm. Sci.* 99, 154–168. <https://doi.org/10.1002/jps.21808>.
- Baird, J.A., Taylor, L.S., 2011. Evaluation and modeling of the eutectic composition of various drug-polyethylene glycol solid dispersions. *Pharm. Dev. Technol.* 16, 201–211. <https://doi.org/10.3109/10837450903584936>.
- Baird, J.A., Van Eerdenbrugh, B., Taylor, L.S., 2010b. A Classification System to Assess the Crystallization Tendency of Organic Molecules from Undercooled Melts. *J. Pharm. Sci.* 99, 3787–3806. <https://doi.org/10.1002/jps.22197>.
- Bansal, K., Baghel, U.S., Thakral, S., 2016. Construction and Validation of Binary Phase Diagram for Amorphous Solid Dispersion Using Flory-Huggins Theory. *AAPS PharmSciTech* 17, 318–327. <https://doi.org/10.1208/s12249-015-0343-8>.
- Bertoni, S., Dolci, L.S., Albertini, B., Passerini, N., 2018. Spray congealing: a versatile technology for advanced drug-delivery systems. *Ther. Deliv.* 9, 833–845. <https://doi.org/10.4155/tde-2018-0049>.
- Bertoni, S., Albertini, B., Ferraro, L., Beggiato, S., Dalpiaz, A., Passerini, N., 2019a. Exploring the use of spray congealing to produce solid dispersions with enhanced indomethacin bioavailability: In vitro characterization and in vivo study. *Eur. J. Pharm. Biopharm.* 139, 132–141. <https://doi.org/10.1016/j.ejpb.2019.03.020>.
- Bertoni, S., Albertini, B., Passerini, N., 2019b. Spray Congealing: An Emerging Technology to Prepare Solid Dispersions with Enhanced Oral Bioavailability of Poorly Water Soluble Drugs. *Molecules* 24. <https://doi.org/10.3390/molecules24193471>.
- Bertoni, S., Albertini, B., Passerini, N., 2020. Different BCS Class II Drug-Gelucire Solid Dispersions Prepared by Spray Congealing: Evaluation of Solid State Properties and In Vitro Performances. *Pharmaceutics* 12. <https://doi.org/10.3390/pharmaceutics12060548>.
- Blasi, P., Casagrande, S., Pedretti, A., Fioretto, D., Vistoli, G., Corezzi, S., 2020. Ketoprofen poly(lactide-co-glycolide) physical interaction studied by Brillouin spectroscopy and molecular dynamics simulations. *Int. J. Pharm.* 580, 119235. <https://doi.org/10.1016/j.ijpharm.2020.119235>.
- Browne, E., Worku, Z.A., Healy, A.M., 2020. Physicochemical Properties of Poly-vinyl Polymers and Their Influence on Ketoprofen Amorphous Solid Dispersion Performance: A Polymer Selection Case Study. *Pharmaceutics* 12. <https://doi.org/10.3390/pharmaceutics12050433>.
- Chen, Z., Liu, Z., Qian, F., 2015. Crystallization of Bifonazole and Acetaminophen within the Matrix of Semicrystalline, PEO–PPO–PEO Triblock Copolymers. *Mol. Pharm.* 12, 590–599. <https://doi.org/10.1021/mp500661v>.
- Forster, A., Hempenstall, J., Tucker, I., Rades, T., 2001. Selection of excipients for melt extrusion with two poorly water-soluble drugs by solubility parameter calculation and thermal analysis. *Int. J. Pharm.* 226, 147–161. [https://doi.org/10.1016/S0378-5173\(01\)00801-8](https://doi.org/10.1016/S0378-5173(01)00801-8).
- Ginés, J.M., Arias, M.J., Moyano, J.R., Sánchez-Soto, P.J., 1996. Thermal investigation of crystallization of polyethylene glycols in solid dispersions containing oxazepam. *Int. J. Pharm.* 143, 247–253. [https://doi.org/10.1016/S0378-5173\(96\)04702-3](https://doi.org/10.1016/S0378-5173(96)04702-3).
- Gue, E., Willart, J.F., Muschert, S., Danede, F., Delcourt, E., Descamps, M., Siepmann, J., 2013. Accelerated ketoprofen release from polymeric matrices: Importance of the homogeneity/heterogeneity of excipient distribution. *Spec. Sect. Formul. Better Med. Child.* 457, 298–307. <https://doi.org/10.1016/j.ijpharm.2013.09.023>.
- Gue, E., Muschert, S., Willart, J.-F., Danede, F., Delcourt-Debruyne, E., Descamps, M., Siepmann, J., 2015. Accelerated ketoprofen release from spray-dried polymeric particles: importance of phase transitions and excipient distribution. *Drug Dev. Ind. Pharm.* 41, 838–850. <https://doi.org/10.3109/03639045.2014.908902>.
- Gupta, M.K., Vanwert, A., Bogner, R.H., 2003. Formation of Physically Stable Amorphous Drugs by Milling with Neusilin. *J. Pharm. Sci.* 92, 536–551. <https://doi.org/10.1002/jps.10308>.
- Law, D., Wang, W., Schmitt, E.A., Long, M.A., 2002. Prediction of Poly(Ethylene) Glycol-Drug Eutectic Compositions Using an Index Based on the van't Hoff Equation. *Pharm. Res.* 19, 315–321. <https://doi.org/10.1023/A:1014499119549>.
- Leuner, C., Dressman, J., 2000. Improving drug solubility for oral delivery using solid dispersions. *Eur. J. Pharm. Biopharm.* 50, 47–60. [https://doi.org/10.1016/S0939-6411\(00\)00076-X](https://doi.org/10.1016/S0939-6411(00)00076-X).
- Lin, X., Hu, Y., Liu, L., Su, L., Li, N., Yu, J., Tang, B., Yang, Z., 2018. Physical Stability of Amorphous Solid Dispersions: a Physicochemical Perspective with Thermodynamic. Kinetic and Environmental Aspects. *Pharm. Res.* 35, 125. <https://doi.org/10.1007/s11095-018-2408-3>.
- Lin, D., Huang, Y., 2010. A thermal analysis method to predict the complete phase diagram of drug–polymer solid dispersions. *Int. J. Pharm.* 399, 109–115. <https://doi.org/10.1016/j.ijpharm.2010.08.013>.
- Mareau, V.H., Prud'homme, R.E., 2005. In-Situ Hot Stage Atomic Force Microscopy Study of Poly(ϵ -caprolactone) Crystal Growth in Ultrathin Films. *Macromolecules* 38, 398–408. <https://doi.org/10.1021/ma0482359>.
- Marsac, P.J., Shamblin, S.L., Taylor, L.S., 2006. Theoretical and Practical Approaches for Prediction of Drug-Polymer Miscibility and Solubility. *Pharm. Res.* 23, 2417. <https://doi.org/10.1007/s11095-006-9063-9>.
- Marsac, P.J., Li, T., Taylor, L.S., 2008. Estimation of Drug-Polymer Miscibility and Solubility in Amorphous Solid Dispersions Using Experimentally Determined Interaction Parameters. *Pharm. Res.* 26, 139. <https://doi.org/10.1007/s11095-008-9721-1>.
- Meere, M., Pontrelli, G., McGinty, S., 2019. Modelling phase separation in amorphous solid dispersions. *Acta Biomater.* 94, 410–424. <https://doi.org/10.1016/j.actbio.2019.06.009>.
- Moseson, D.E., Taylor, L.S., 2018. The application of temperature-composition phase diagrams for hot melt extrusion processing of amorphous solid dispersions to prevent residual crystallinity. *Int. J. Pharm.* 553, 454–466. <https://doi.org/10.1016/j.ijpharm.2018.10.055>.

- Nair, A.R., Lakshman, Y.D., Anand, V.S.K., Sree, K.S.N., Bhat, K., Dengale, S.J., 2020. Overview of Extensively Employed Polymeric Carriers in Solid Dispersion Technology. *AAPS PharmSciTech* 21, 309. <https://doi.org/10.1208/s12249-020-01849-z>.
- Ogieglo, W., Wessling, M., Benes, N.E., 2014. Polymer Relaxations in Thin Films in the Vicinity of a Penetrant- or Temperature-Induced Glass Transition. *Macromolecules* 47, 3654–3660. <https://doi.org/10.1021/ma5002707>.
- Paberit, R., Rilby, E., Göhl, J., Swenson, J., Refaa, Z., Johansson, P., Jansson, H., 2020. Cycling Stability of Poly(ethylene glycol) of Six Molecular Weights: Influence of Thermal Conditions for Energy Applications. *ACS Appl. Energy Mater.* 3, 10578–10589. <https://doi.org/10.1021/acsaem.0c01621>.
- Panini, P., Rampazzo, M., Singh, A., Vanhoutte, F., Van den Mooter, G., 2019. Myth or Truth: The Glass Forming Ability Class III Drugs Will Always Form Single-Phase Homogenous Amorphous Solid Dispersion Formulations. *Pharmaceutics* 11. <https://doi.org/10.3390/pharmaceutics11100529>.
- Paudel, A., Worku, Z.A., Meeus, J., Guns, S., Van den Mooter, G., 2013. Manufacturing of solid dispersions of poorly water soluble drugs by spray drying: Formulation and process considerations. *Poorly Soluble Drugs* 453, 253–284. <https://doi.org/10.1016/j.ijpharm.2012.07.015>.
- Prudic, A., Ji, Y., Sadowski, G., 2014. Thermodynamic Phase Behavior of API/Polymer Solid Dispersions. *Mol. Pharm.* 11, 2294–2304. <https://doi.org/10.1021/mp400729x>.
- Thakral, S., Thakral, N.K., 2013. Prediction of Drug-Polymer Miscibility through the use of Solubility Parameter based Flory-Huggins Interaction Parameter and the Experimental Validation: PEG as Model Polymer. *J. Pharm. Sci.* 102, 2254–2263. <https://doi.org/10.1002/jps.23583>.
- Tian, Y., Booth, J., Meehan, E., Jones, D.S., Li, S., Andrews, G.P., 2013. Construction of drug-polymer thermodynamic phase diagrams using Flory-Huggins interaction theory: identifying the relevance of temperature and drug weight fraction to phase separation within solid dispersions. *Mol. Pharm.* 10 (1), 236–248.
- Unga, J., Matsson, P., Mahlin, D., 2010. Understanding polymer–lipid solid dispersions—The properties of incorporated lipids govern the crystallisation behaviour of PEG. *Int. J. Pharm.* 386, 61–70. <https://doi.org/10.1016/j.ijpharm.2009.10.049>.
- Van Duong, T., Goderis, B., Van Humbeeck, J., Van den Mooter, G., 2018. Microstructure of Pharmaceutical Semicrystalline Dispersions: The Significance of Polymer Conformation. *Mol. Pharm.* 15, 629–641. <https://doi.org/10.1021/acs.molpharmaceut.7b01007>.
- Van Duong, T., Van den Mooter, G., 2016. The role of the carrier in the formulation of pharmaceutical solid dispersions. Part I: crystalline and semi-crystalline carriers. *Expert Opin. Drug Deliv.* 13, 1583–1594. <https://doi.org/10.1080/17425247.2016.1198768>.
- Van Duong, T., Van Humbeeck, J., Van den Mooter, G., 2015. Crystallization Kinetics of Indomethacin/Polyethylene Glycol Dispersions Containing High Drug Loadings. *Mol. Pharm.* 12, 2493–2504. <https://doi.org/10.1021/acs.molpharmaceut.5b00299>.
- Vueba, M.L., Pina, M.E., Veiga, F., Sousa, J.J., de Carvalho, L.A.E.B., 2006. Conformational study of ketoprofen by combined DFT calculations and Raman spectroscopy. *Int. J. Pharm.* 307, 56–65. <https://doi.org/10.1016/j.ijpharm.2005.09.019>.
- Wu, Q., Kennedy, M.T., Nagapudi, K., Kiang, Y.-H., 2017. Humidity induced phase transformation of poloxamer 188 and its effect on physical stability of amorphous solid dispersion of AMG 579, a PDE10A inhibitor. *Int. J. Pharm.* 521, 1–7. <https://doi.org/10.1016/j.ijpharm.2017.01.059>.
- Yang, M., Gogos, C., 2013. Crystallization of poly(ethylene oxide) with acetaminophen – A study on solubility, spherulitic growth, and morphology. *Eur. J. Pharm. Biopharm.* 85, 889–897. <https://doi.org/10.1016/j.ejpb.2013.03.025>.
- Yu, C., Xie, Q., Bao, Y., Shan, G., Pan, P., 2017. Crystalline and Spherulitic Morphology of Polymers Crystallized in Confined Systems. *Crystals* 7. <https://doi.org/10.3390/cryst7050147>.
- Zhang, Z., Li, Q., Yesildag, C., Bartsch, C., Zhang, X., Liu, W., Loebus, A., Su, Z., Lensen, M.C., 2018. Influence of Network Structure on the Crystallization Behavior in Chemically Crosslinked Hydrogels. *Polymers* 10, 970. <https://doi.org/10.3390/polym10090970>.
- Zhang, Z., Dong, L., Guo, J., Li, L., Tian, B., Zhao, Q., Yang, J., 2021. Prediction of the physical stability of amorphous solid dispersions: relationship of aging and phase separation with the thermodynamic and kinetic models along with characterization techniques. *Expert Opin. Drug Deliv.* 18, 249–264. <https://doi.org/10.1080/17425247.2021.1844181>.
- Zhu, Q., Taylor, L.S., Harris, M.T., 2010. Evaluation of the Microstructure of Semicrystalline Solid Dispersions. *Mol. Pharm.* 7, 1291–1300. <https://doi.org/10.1021/mp1000907>.
- Zhu, Q., Harris, M.T., Taylor, L.S., 2012. Modification of Crystallization Behavior in Drug/Polyethylene Glycol Solid Dispersions. *Mol. Pharm.* 9, 546–553. <https://doi.org/10.1021/mp200546p>.